Additive Manufacturing 44 (2021) 102023

Contents lists available at ScienceDirect

Additive Manufacturing

journal homepage: www.elsevier.com/locate/addma

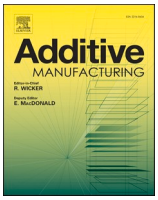

Rubber ink formulations with high solid content for direct-ink write process

Myoeum Kim, Jae-Won Choi *

Department of Mechanical Engineering, The University of Akron, 244 Sumner St, Akron, OH 44325-3903, USA

ARTICLE INFO

Keywords:
Natural rubber
Vulcanization
Direct ink write
Direct-print
High solid content

ABSTRACT

Additive manufacturing (AM) is a potential technology for future applications such as smart devices and airless tires. Natural rubber, which is used with restricted processing methods in the tire industry, has drawbacks for use in AM technology because of the high pressure and temperatures required to process it. The motivation of this study is to determine if natural rubber can be used as a 3D printable material. To this end, natural rubber latex (NL) was used as the basis for a printable ink. Liquid rubber was introduced to the NL in various amounts to increase the amount of solid in the ink so as to improve its 3D printability and prevent shrinkage, and sulfur and other additives were incorporated into the mixture to facilitate vulcanization. The rheological properties of inks were investigated for consistent extrusion as well as for shape retention in the printed parts. Dimensional accuracy, printability, and mechanical properties of 3D printed specimens have been investigated. Using a direct-print AM system and the developed rubber ink, various 3D structures were fabricated to demonstrate that the developed ink could be a candidate for future rubber applications.

1. Introduction

Natural rubber, which is extracted from rubber trees, is used in more than 40,000 products, including surgical gloves, toys, clothes, vehicle tires, and medical devices [1]. Natural rubber has high strength and can be stretched in multiple directions without breaking. Because synthetic rubber cannot match these properties, it cannot be used as a substitute for natural rubber in most products. Current research on natural rubber includes the study of various composites [2], the vulcanization process [3], environmental impacts [4], the devulcanization process [5], and the mechanical properties of natural rubber [6].

Natural rubber latex (NL) is composed of ~45% *cis*-isoprene, ~5% non-rubber content (such as carbohydrates and protein), and ~50% water by weight. Raw natural rubber is classified as a polymer, as it contains large molecules composed of many smaller molecules of the same kind. Raw natural rubber generally includes four different isomers of polyisoprenes, and it has a molecular weight that is several times higher than most synthetic rubbers [7]. Whereas synthetic rubber is produced from isoprene monomers [8], natural raw rubber is formed as a result of a biochemical reaction from isopentenyl pyrophosphate that occurs in the rubber tree. The latex state of natural rubber includes colloids that are formed during the coagulation and drying process in an industrial setting, and the latex is produced as a sheet. This rubber sheet needs high temperature and pressure to entangle numerous rubber chains in the rubber sheet during processing [9]. The loss of weight and the physical properties of the resulting materials need to be considered when processing NL due to the presence of water. Therefore, various processing methods (e.g., manufacturing processes and pre-treatments) and additives (e.g., synthetic rubber) [10] can be considered as candidates for enhancing the dimensional accuracy of the resulting part or component [11].

Additive manufacturing (AM), also called 3D printing, was introduced in the 1980's, and its application has been investigated for aerospace [12], automotive [13,14], and architectural [15] applications. In industry, the AM technique has been used for not only the design iterations by prototyping but producing actual parts and devices, since it allows customized manufacturing without a mold and does not require expensive tools [16]. AM materials used include metals [17,18], ceramics [19,20], polymers [21–23], and composites [24]. The printing materials can take various forms (such as a filament [25], a powder [26], or an ink [27,28]), depending on the selected 3D printing process. In AM processes that use solid filaments, a filament is extruded after melting at high temperature, and many types of solid polymer filaments (such as polylactic acid (PLA) [29], acrylonitrile butadiene styrene (ABS) [30], and nylon [31]) are used as printing materials. In addition, paste-type materials with thixotropic properties (i.e., time-dependent shear thinning properties) have been widely used in direct ink write (DIW)—which is also known as direct-print (DP) and direct-write (DW) [32]—

* Corresponding author.
E-mail address: jchoi1@uakron.edu (J.-W. Choi).

https://doi.org/10.1016/j.addma.2021.102023
Received 11 March 2021; Received in revised form 23 April 2021; Accepted 23 April 2021
Available online 15 May 2021

due to the high flexibility in the choice of materials.

Although AM processes are mature technologies, real rubber compounds with high solid content have not been used in AM, whereas rubber-like polymers or elastomers (including TangoPlus [32], NinjaFlex [34], PRO Series Flex [35], and PolyFlex™ [36], among others) are widely used for this purpose. The rubber compound currently used in the tire industry is a possible candidate material for AM, but this material has limitations for AM applications because of the high pressure and high temperatures that are required to process it. In recent years, Maria et al. showed the capability of printing elastomeric latex materials using an inkjet process [37], and Miguel et al. printed natural rubber latex using a customized inkjet printer [38]. While these studies demonstrated that inkjet printing of latex could be achieved by controlling the material's viscosity, the use of latex has several drawbacks (such as nozzle clogging and agglomeration). Moreover, the inks used in the inkjet method are required to solidify and cure quickly before the printed patterns are deformed. Philip et al. printed synthetic latex using a vat photopolymerization printing method [39] in which scaffold monomers were used to form a supporting hydrogel scaffold around the latex particles. However, the technique still has limitations in terms of the polymer used in the photo-curing process and the narrow range of viscosity for the printing material. In addition, this material involves significant shrinkage of ~40 vol% because of a large amount of the solvent in latex although they are photo-polymerized. Rubber inks with high solid content that can be used in a DP process have not yet been developed, which is the motivation of this research. Various post-processing methods can be accompanied with a DP process such as photopolymerization [32], drying [40], and sintering [41], where vulcanization has been suggested in this study.

In this study, NL was selected as the matrix for a rubber ink that is suitable for use in the DP process. To increase the amount of solids in the latex, different ratios of synthetic liquid rubber were incorporated. Various tests were conducted to verify the solid content and optimize the print parameters, and structures were printed to demonstrate the feasibility of using the developed ink for AM.

2. Materials and methods

The research program in this study investigated the rheological properties prepared rubber inks and characterized them made from NL as well as inks that incorporated various ratios of natural latex and liquid rubber—ranging from an ink with no liquid rubber (BN-0) to inks containing increasingly higher proportions of liquid rubber (BN-1, BN-2, and BN-3). The rheological properties for each ink formulation were investigated, and the line widths for rubber inks printed at various speeds and under various amounts of pressure were measured in order to optimize the printing parameters for each ink. Using the optimized parameters, 3D-printed specimens for each ink formulation were fabricated using DP and were heat-treated to induce vulcanization, and the mechanical properties and dimensional accuracies of the resulting components were compared. Fig. 1 presents a summary of the test procedures conducted in this study, and the sections below provide additional details about the materials, the formulation of the various rubber inks, and the test setup and printing process used for 3D printing of the rubber inks.

2.1. Materials

The natural rubber latex used in this study was purchased from Liquid Latex Direct (Burton-upon-Stather, UK), while the liquid butadiene rubber (which was based on an acrylate oligomer) was obtained from Kuraray Company, Ltd (Tokyo, Japan). TritonX-100 surfactant and stearic acid activator were purchased from Sigma-Aldrich (St. Louis, USA). The vulcanizing agents and accelerators used in this study—sulfur, zinc oxide, tetramethylthiuram disulfide (TMTD), and N-cyclohexyl-2-benzothioazole sulfenamide (CBTS) —were provided by Akrochem Corp (Akron, USA).

Thermogravimetric analysis (TGA) was used to measure the thermal decomposition behavior of the NL and characterize the amount of natural rubber solids in the raw latex. In this analysis, which was conducted using a TA Instruments Q500 thermogravimetric analyzer, natural rubber latex samples were heated from 25 °C to 600 °C at a scanning rate of 10 °C/min in a nitrogen atmosphere. The analysis showed the initial solid content of the raw NL to be approximately 60% (Fig. 2). In an effort to increase the amount of solids in the latex (so as to enhance the dimensional accuracy of components printed with NL by reducing shrinkage due to the evaporation of non-solid content), it was necessary to reduce the amount of water. To accomplish this, the raw NL was centrifuged using an Allegra X-30R series centrifugal separator from Beckman Coulter, Inc., and the latex was collected from the surface of the water; this process was repeated two times. The collected latex was

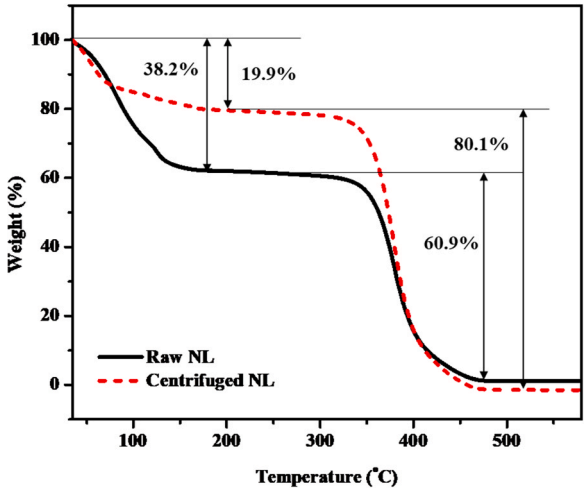

Fig. 2. Thermogravimetric analysis data for raw and centrifuged NL.

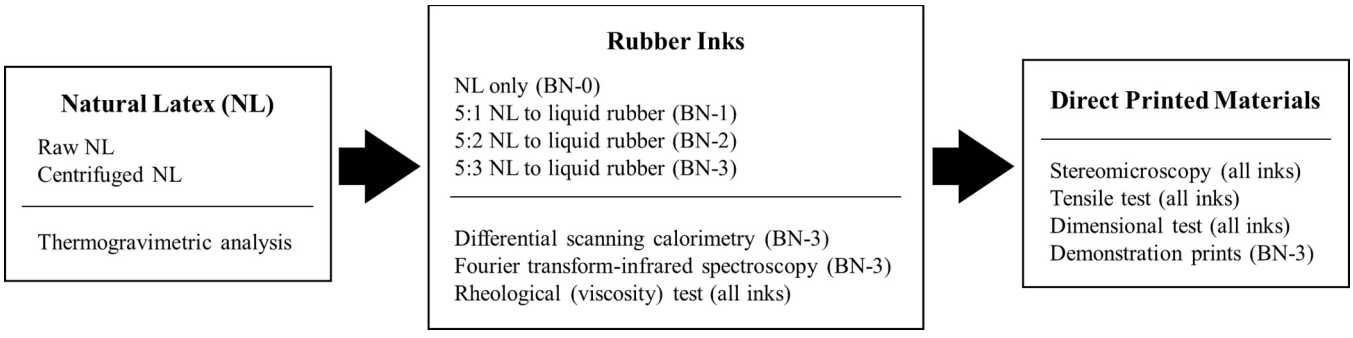

Fig. 1. Summary of the testing program used in this study.

then blended at 2500 rpm for 30 s in a FlackTek SpeedMixer™ high-speed mixer. Thermogravimetric analysis revealed that the centrifuged natural latex had a solid content of approximately 80% (Fig. 2), which was deemed to be sufficient for DP.

2.2. Preparation of rubber inks

Before using the natural latex in the preparation of rubber inks, the centrifuged NL was first filtered through a nylon net filter with a 100-μm pore mesh (Sigma-Aldrich) to remove any agglomerated particles. A portion of the centrifuged and filtered NL was kept aside for printing and was designated as a base matrix for ink BN-0. To a container that contained the remaining filtered natural latex, liquid synthetic butadiene rubber (liquid rubber) was added to obtain mixtures having different ratios of NL to synthetic rubber (5:1, 5:2 and 5:3, which were designated as base matrixs for inks BN-1, BN-2, and BN-3, respectively). Next, in order to prepare the final rubber inks called as BN-0, BN-1, BN-2, and BN-3, 2 per hundred rubber (phr) of Triton™ X-100 surfactant was added to the base matrixes composed by NL and NL/liquid rubber mixtures, and each ink was mixed in the high-speed mixer with ceramic beads at 2500 rpm for 30 s. To facilitate the vulcanization of the inks after printing, 2 phr of sulfur and 1 phr of stearic acid were added, and each ink mixture was again blended in the high-speed mixer at 2500 rpm for 30 s. Next, 4 phr of zinc oxide, 1 phr of TMTD, and 4 phr of CBTS were added, and each mixture was blended again at 2500 rpm for 30 s. Each ink mixture was then filtered through a mesh with a pore diameter of 140 μm to remove large aggromerates.

With the assumption that there was no significant change in their compositions after filtration, solid content was calculated from the ink formulations of on the four rubber inks. The results, which are presented in Table 1, show that the solid content of the rubber inks ranged between 82.0% (for the ink made using NL only) and 88.9% (for the ink that incorporated the largest amount of liquid rubber).

2.3. Setup and printing process for the direct-print system

The setup for the customized DP system used in this study [32] (Fig. 3) consists of a dispensing system (pressure controller, syringes, and their holders) and motorized xyz-stage. A precision position control of the syringe tip was enabled by a PRO115 high-resolution XYZ linear stage (Aerotech, Inc.). ThorLabs model XR35C/M manual translation stages were installed on the Z-stage to calibrate the gap distance between the substrate and the dispensing tips. Extrusion through the syringe was accomplished through the application of pressure by a Ultimus™ I pneumatic pump (Nordson EFD). The XYZ linear stages and pressure controller were synchronized using G-code instructions and were interfaced with *LabVIEW* software (National Instruments).

A file in stereolithography (STL) format was prepared from a 3D model designed using *SolidWorks*® computer-aided design (CAD) software. Open-source software (*Repetier-Host*; Hot-World GmbH) was used to convert the STL file into layers and generate the G-code instructions that contain the toolpath and extrusion parameters needed for 3D printing. The layer thickness for the print was adjusted based on a tip size of 250 μm. A 100% infill density and a 45°/45° raster angle were used for the print settings. Each rubber ink was loaded into an Optimum® syringe barrel (Nordson EFD) immediately after preparation to prevent drying, then re-mixed using a high-speed mixer for 30 s at 2500 rpm to remove any air bubbles in the material. Next, the syringe was placed on the XYZ stage and connected to the pneumatic pump for 3D printing. Various pressure and speed ranges were investigated to optimize the printing parameters for the four inks.

Table 1
Solid content of 3D printing inks used to print samples.

Ink	Weight ratio (NL to Liquid Rubber)	Final Solid Content (% weight)
BN-0	NL only	82.0
BN-1	5:1	85.1
BN-2	5:2	87.2
BN-3	5:3	88.9

3. Results and discussion

3.1. Vulcanization process

xAn aqueous phase of NL was used to print samples of rubbers having high molecular weights. Latex was centrifuged and obtained as a viscous latex with solid content that was high enough to allow the material to be used to print a 3D structure using DP. Fig. 4 illustrates the processing design of vulcanization. Liquid rubber, which is used to enhance the solid content of the latex, is uniformly embedded to the centrifuged latex, which serves to form a supporting scaffold around the latex particles. Additives were then incorporated into the mixture. The high viscosity of the blended mixture enabled the additives (sulfur, stearic acid, zinc oxide, TMTD, and CBTS) to diffuse uniformly throughout the latex. Vulcanization of the material was then achieved by thermal treatment of the rubber ink sample at 160 °C for 20 min

The curing condition and mechanism were investigated to understand vulcanization process. In this study, curing was investigated by conducting two different tests using rubber ink BN-3, which was the ink having the highest solid content.

Differential scanning calorimetry (DSC) was conducted with a TA Instruments Q200 differential scanning calorimeter to measure the vulcanization temperature of the rubber. A small amount of rubber ink (5–10 mg) was placed in a DSC pan and heated from −50–170 °C for two cycles at scanning rates of 5, 8, and 10 °C/min. The curing temperature based on various heating rates of BN-3 was determined using the DSC result, as shown in Fig. 5. The broad exothermic peak at the heating rate of 5 °C/min on the DSC scan was observed at temperatures ranging from 120° to 130 °C. The cross-linking is known to discharge a quantum of energy, driving an exothermic reaction [42]. Exothermic peaks were not observed in the subsequent heating scans, indicating that the carbon double bonds on the rubber chain were completely crosslinked by sulfur during the first cycle. The peaks for BN-3 at heating rates of 5 °C/min, 8 °C/min, and 10 °C/min appeared at 127.88 °C, 137.70 °C, and 142.86 °C, respectively. An isothermal reaction was predicted as the reaction peaks were shifted to higher temperatures at higher heating rates since the reaction kinetics depend on the heating rate [43].

Fourier transform infrared spectroscopy (FTIR) was conducted on the rubber ink BN-3 and a vulcanized rubber compound of the same ink to confirm the successful vulcanization and crosslinking of the rubber chains with sulfurs. The characterization was performed with a Bruker ALPHA II compact FTIR spectrometer using a wavelength range of 500–4000 cm^{-1}, and the resulting spectra were used to verify if the synthesis reaction in the vulcanization process was complete and verify if a structural change of natural rubber and liquid rubber had occurred, according to the change in the monomer ratio. As shown in the FTIR spectra presented in Fig. 6, the characteristic peak of the carbon double bond at 1640 cm^{-1} became smaller after vulcanization as compared to the double peaks at 2800 cm^{-1} in the FTIR spectrum for rubber ink BN-3, indicating that carbon double bonds were vulcanized by the sulfur. In addition, the peak for the hydroxy group of water at 3400 cm^{-1} disappeared, indicating that the water in latex had fully evaporated.

3.2. Rheological properties

A TA Instruments ARES G2 rheometer was used under a strain rate from 200 to 0.01 s^{-1} at room temperature to measure the viscosity of the four rubber inks. The results for rheological testing are presented in Fig. 7. As can be noticed from this figure, the viscosity of the rubber ink depends on the shear strain, which is an important rheological property for improving the printing quality of the ink. The high viscosity of the 3D

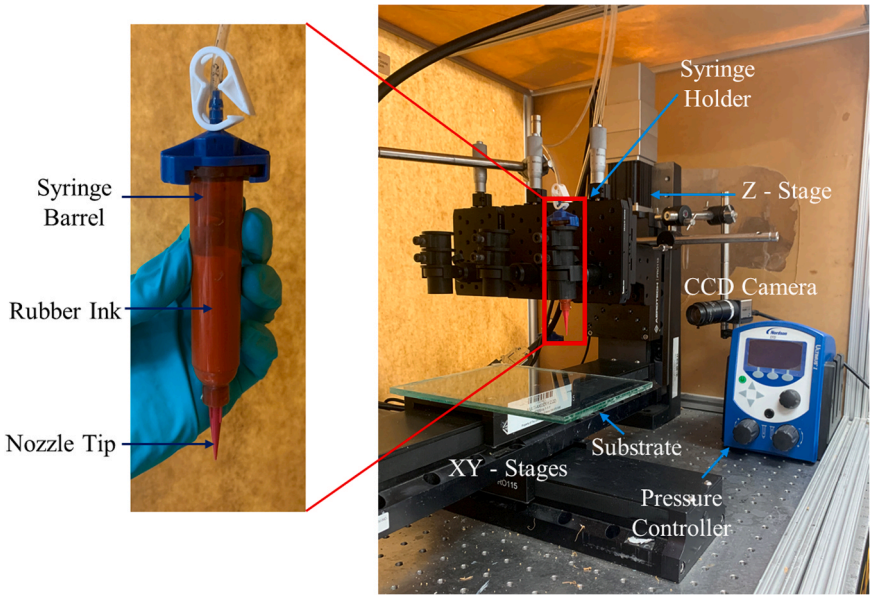

Fig. 3. Direct-print system.

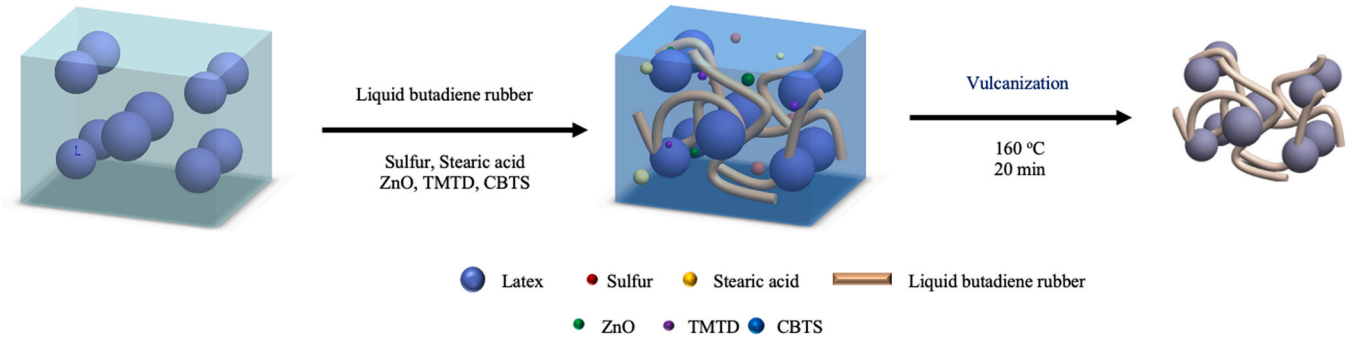

Fig. 4. Schematic diagram showing the incorporation of liquid rubber and additives to form blended rubber inks and the results of the vulcanization process.

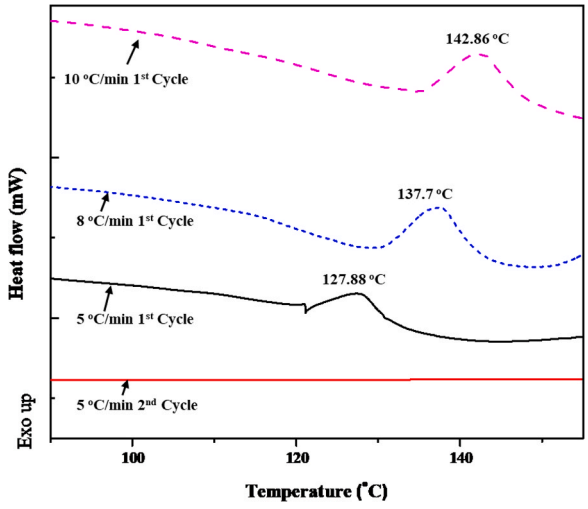

Fig. 5. The first and second cycles of the vulcanization process for rubber ink BN-3 in the DSC analysis.

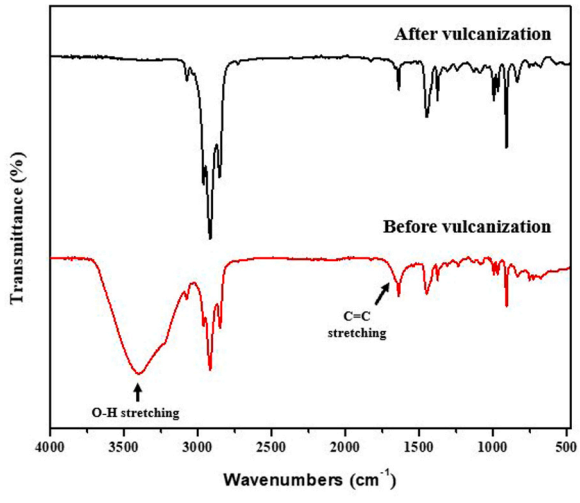

Fig. 6. FTIR spectra for unvulcanized and vulcanized BN-3 ink.

printable ink enabled the printed sample to hold its shape after extrusion from the nozzle tip, when the ink is no longer being subjected to external stress. This reflects the shear-thinning property of non-Newtonian fluids, in which the fluid viscosity decreases with the increase in shear stress [33]. As shown in Fig. 7, the viscosities of the four ink materials were measured at shear rates from 0.001 to 200 s^{-1}. The yield viscosities for BN-0, BN-1, BN-2, and BN-3 were 197,591 Pa·s, 159,617 Pa·s, 123, 174 Pa·s, and 130,718 Pa·s, respectively, where the initial viscosities under no shear strain were 41,230 Pa·s, 30,337 Pa·s, 22,179 Pa·s, 25,

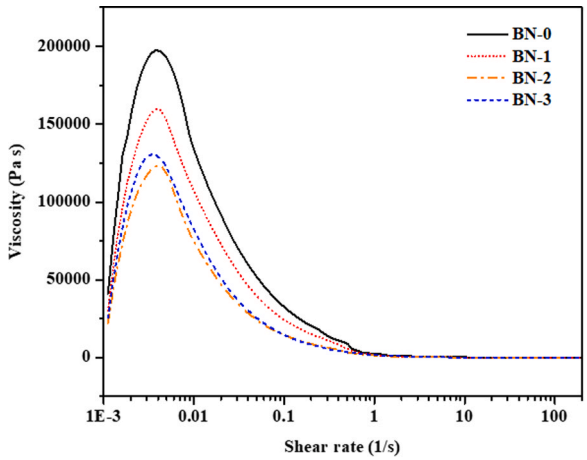

Fig. 7. Rheology test results for rubber inks conducted at room temperature.

458 Pa·s, respectively.

The liquid butadiene rubber incorporated into the NL has a molecular weight of 5500 and a viscosity of 5.5 Pa·s, which enables it to progressively lower the yield viscosity of inks BN-1, BN-2, and BN-3 by increasing the amount of liquid rubber. The viscosity change for BN-1, BN-2, and BN-3 reaches the yield viscosity from the lower value (which indicates shear thickening) because all inks (including NL) have a colloidal suspension state, where the non-flocculated state was transited to a state of flocculation under shear stress [44]. Lastly, the inks flow at a high shear rate as the chains of the rubber molecules start to disentangle and align along the direction of shear so that the viscosities of the inks significantly decreased (216 Pa·s, 127 Pa·s, 135 Pa·s, 138 Pa·s for BN-0, BN-1, BN-2 and BN-3, respectively) [45].

3.3. Printability test of composite inks

In order to obtain the appropriate printing parameters for the four rubber inks, a printability test was conducted by operating the DP system using various printing pressures and speeds to print ink materials BN-0, BN-1, BN-2, and BN-3. The inks were continuously printed for a

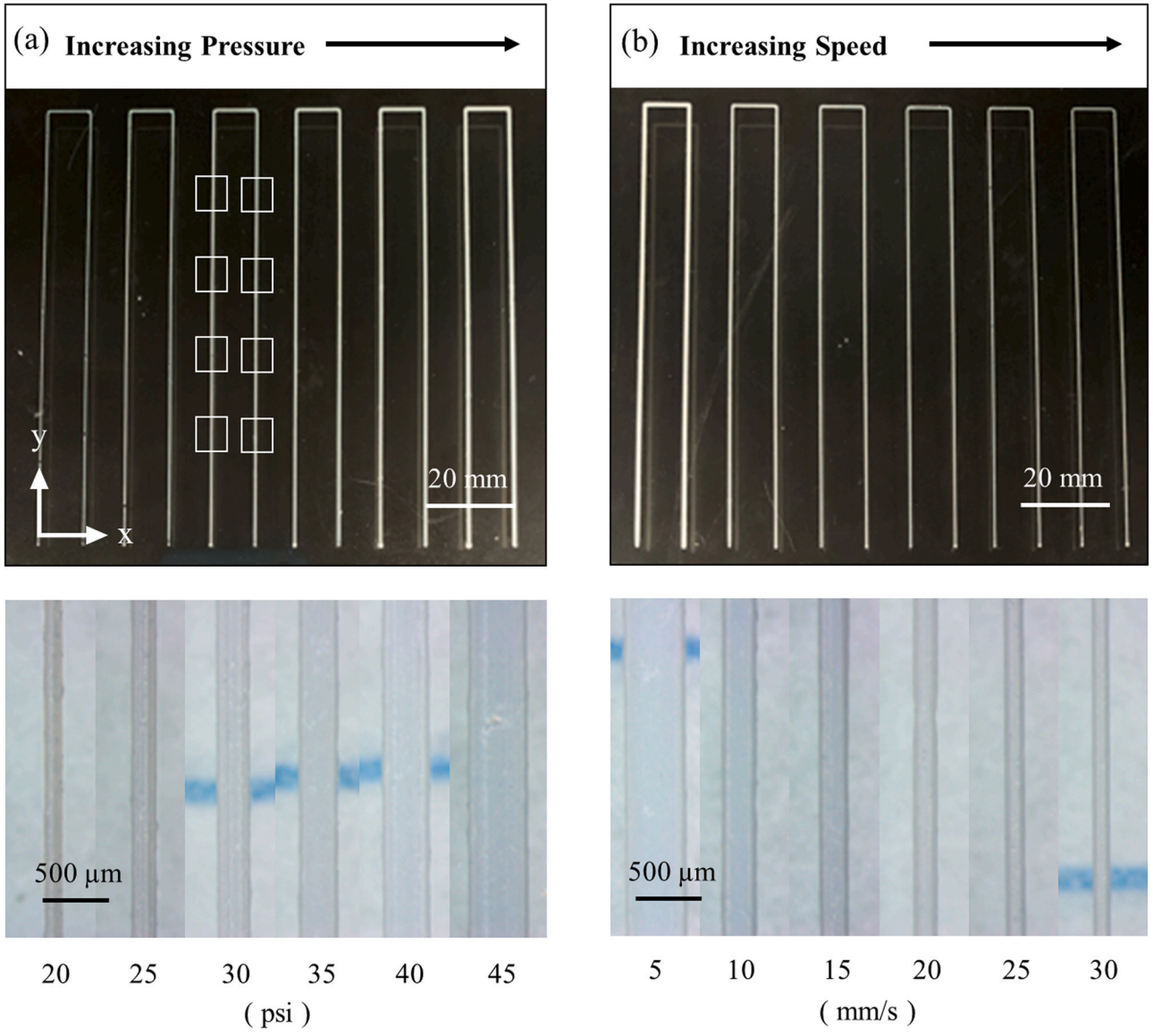

Fig. 8. Microscope images of printed lines for rubber ink BN-3 (a) under various pressures at a constant speed of 15 mm/s and (b) at various speeds under a constant pressure of 20 psi.

length of 150 mm in the positive Y-direction and 150 mm in the negative Y-direction, with a distance of 10 mm between lines (along the X-direction). The gap height between the nozzle tip and substrate was set at 225 μm, which is 90% of the nozzle diameter. To enable the line width at the same location to be measured consistently, four parallel lines were drawn in the X-direction (against the printing direction) on a piece of paper, and the paper was attached to the bottom of the glass substrate so that the drawn lines would be visible in the background. The four parallel lines were drawn on the paper intersected with the two lines printed in the Y-direction, creating four intersection points in each direction (for a total of eight points on the two printed lines). This enabled the line width measurements for each ink to be conducted at the same eight locations on the printed lines.

A Zeiss SteREO Discovery V12 stereomicroscope was used to measure the width of lines printed using the four rubber inks. The results for rubber ink BN-3 (the ink with the highest solid content) at each pressure and speed combination are shown in Fig. 8. Fig. 8a shows six sets of lines of BN-3 ink printed at pressures ranging from 20 to 45 psi in 5-psi increments at a constant speed of 15 mm/s. The BN-3 ink began to continuously dispense from the nozzle at 20 psi with an average line width of 128 μm, which is 50% of the nozzle diameter. At 30 psi, the printed line width reached an average value of about 260 μm, which is slightly more than 100% of the nozzle diameter. Fig. 8b shows the six sets of lines printed at speeds ranging from 5 to 30 mm/s in 5-mm/s increments at a constant pressure of 20 psi. Rubber ink BN-3 had an average line width that was about 200% of the nozzle diameter at a speed of 5 mm/s. At speeds between 10 and 15 mm/s, the width of the line was nearly equal to the nozzle diameter. BN-3 began to print without discontinuities at 30 mm/s, where it showed an average line width of 146 μm (which is 58.4% of the nozzle diameter).

Fig. 9 shows the relationship between the line width and the print parameters. Because the different ink material compositions (BN-0, BN-1, BN-2 and BN-3) have different yield viscosity values, different pressure levels and printing speeds were required to print each ink material. As shown in Fig. 9a, the pressure was fixed at 20 psi (the minimum pressure required for the extrusion for all four ink materials), and the line width was measured at printing speeds from 5 to 30 mm/s in increments of 5 mm/s. At the initial speed of 5 mm/s, the line widths for BN-0, BN-1, BN-2, and BN-3 were 400%, 400%, 300%, and 200% of the nozzle diameter, respectively. From the results shown in Fig. 9b, it can be seen that the line width is dependent on the pressure, which began at either 17 or 20 psi (depending on which ink was used for the print) and was increased to 45 psi in increments of 5 psi at a fixed printing speed of 15 mm/s (the speed that was found to be the optimum condition for printing rubber ink BN-3). The width of the lines printed using rubber inks BN-0, BN-1, and BN-2 were about 700%, 600%, and 500% of the nozzle diameter, respectively, at a pressure of 45 psi. The line width for rubber ink BN-3, the material combination that included the largest amount of liquid rubber, was about 200% of the nozzle diameter, which is a relatively small change in width as compared to that for the lines of other inks at 45 psi.

The printing parameters are based on the rheological properties of the material, which are related to the amount of liquid rubber incorporated into the ink. The line width of the material having the largest amount of liquid rubber (BN-3) showed no significant changes even when the material was printed at a wide range of pressures and scanning speeds. This occurred because the liquid rubber remains sticky even though viscosity is low (about 5.5 Pa·s), and the adhesion prevents the ink from spreading during the printing. Based on the pressure and speed tests, the optimum print settings were chosen for printing the rubber inks: the speed was set at 15 mm/s for all four inks, and pressures of 19 psi, 24 psi, 18 psi, and 30 psi were applied for BN-0, BN-1, BN-2, and BN-3, respectively.

3.4. Dimensional accuracy analysis

In the DP process for building a 3D structure, one of the most important factors that define the printability of a newly developed material is the dimensional accuracy of the produced part. The principle for accuracy assessment in this study is to evaluate the dimension of each edge of the as-produced (green) part and a vulcanized part. The 3D model of a cube structure used for accuracy tests, which was designed as a 1 cm^3 unicube using *SolidWorks*® (Fig. 10a), was printed using 250-μm nozzle tip with 100% infill density (Fig. 10b). Five cube specimens for each ink were printed for testing. Fig. 10c shows the printed green part of the cube and the vulcanized specimen, where the inserted image demonstrates the XYZ direction of the cube. The dimensions of each green part were measured using low force calipers. The average volume changes for BN-0, BN-1, BN-2, and BN-3 (Fig. 11a–d) were −12.49%, −7.52%, −5.47%, and −4.69%, respectively. From this figure, it can be noticed that the volume of the printed part was lower following vulcanization. The results also show that the average change in volume was smaller when the solid content in the ink was increased. This finding was attributed to the evaporation of water from the inks through heat treatment, as shown in the FTIR spectra in Fig. 6. The space that was previously filled with water was emptied by evaporation, resulting in shrinkage of the entire structure.

3.5. Tensile testing

Unidirectional tensile tests on specimens prepared by all four inks (BN-0, BN-1, BN-2, and BN-3) were conducted to investigate the effect of the amount of liquid rubber in the ink on the tensile properties of a printed rubber compound. A total of 16 ASTM D638 Type V dogbone

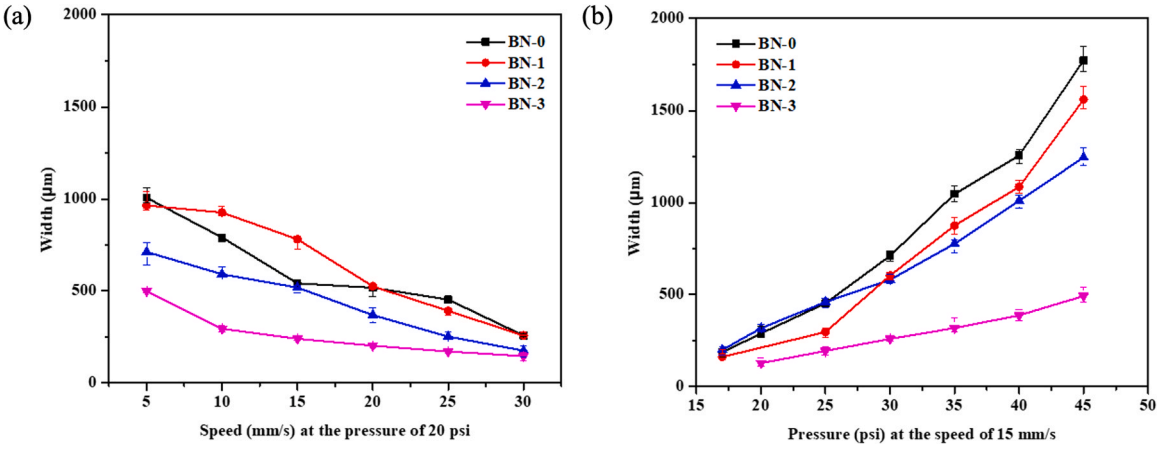

Fig. 9. Correlation between the width of the printed lines and the print parameters (a) at various speeds and (b) under various pressures.

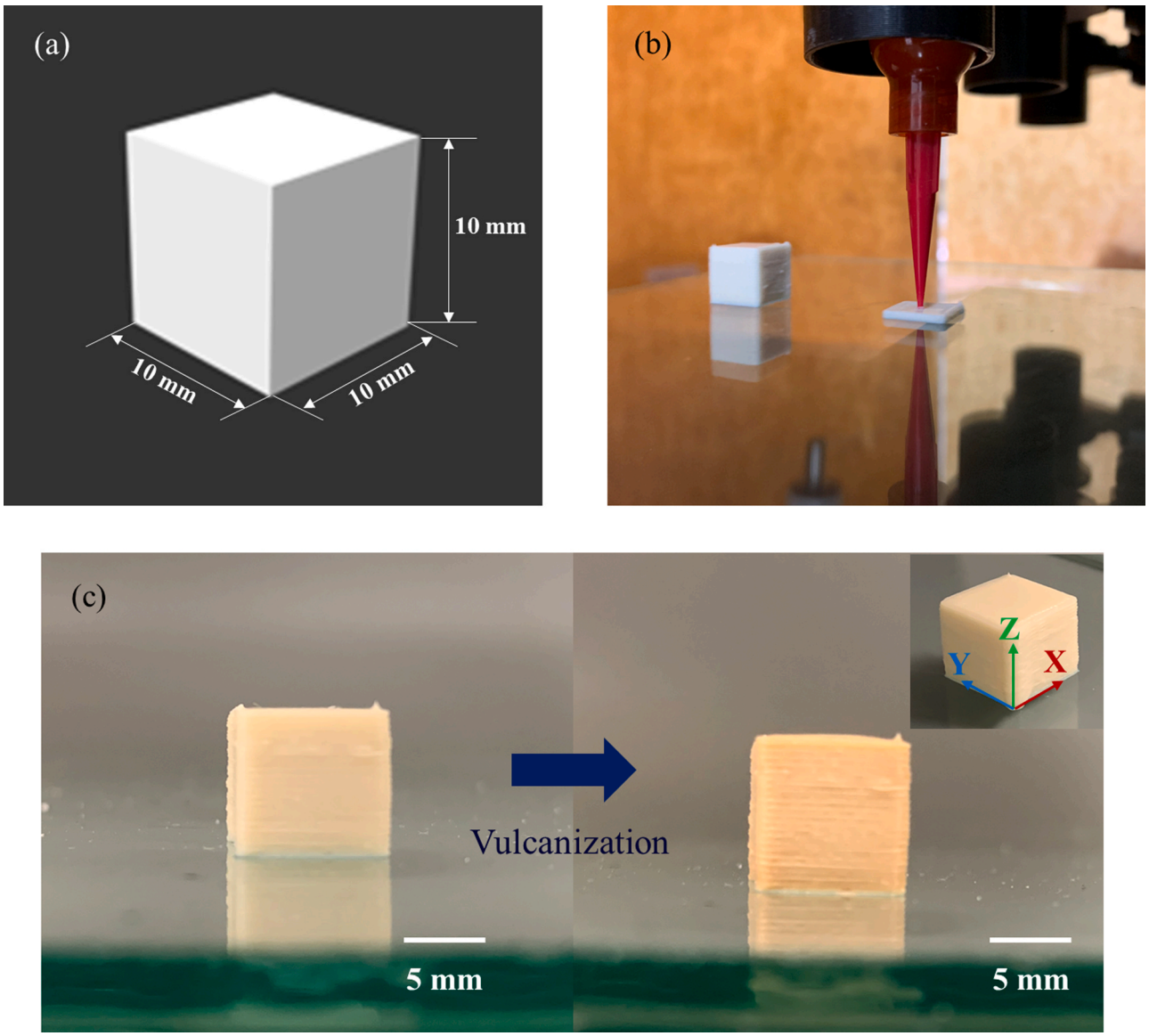

Fig. 10. Dimemsional accuracy experiments: (a) 3D model of cube with dimensions, (b) printing of the model, and (c) a comparison of a printed cube of BN-3 before and after the vulcanization process.

specimens (four specimens for each ink) were 3D printed using DP, where the design of the specimen had a 100% infill density and where a nozzle with a diameter of 250 μm was used for printing. Fig. 12 presents the 3D model of the tensile test specimen and an image showing the printing of the specimen. Once the specimens were successfully printed, they were fully vulcanized by heating at 160 °C for 20 min prior to mechanical testing.

An Instron UTS 5582 universal testing machine was used to conduct tensile tests on the 3D-printed dogbone specimens at a speed of 5 mm/s. Tensile testing was accomplished for specimens of all four rubber inks, and stress–strain curves were obtained (Fig. 13). The averaged maximum tensile stresses of the specimens for BN-0, BN-1, BN-2, and BN-3 were 16.5 MPa, 4.0 MPa, 0.6 MPa, 0.4 MPa, respectively. Rubber ink BN-0, which contains no liquid rubber, was stretched to 418.4%, while BN-1, BN-2, and BN-3 were stretched to 278.6%, 48.5%, and 32.2%, respectively. The results show that the tensile stress decreases as the amount of liquid rubber increases. This is because liquid butadiene rubber consists of low molecular chains, resulting in lower mechanical strength. In addition, since natural rubber and liquid rubber are cross-linked separately, the interface between rubbers could be a weaker point during extension.

3.6. Demonstration of 3D structures printed using rubber ink

Different 3D structures were fabricated by the DP process to demonstrate the capabilities of the prepared rubber ink. The structures were built using ink BN-3 (the composite rubber ink with the highest solid content) using the printing parameters obtained from the printability test discussed in Section 3.3. Fig. 14 shows the process for manufacturing 3D designs of letter forms, an inclined gear part, and a tire tread. CAD models of the 3D structures were first designed in *SolidWorks*® (Fig. 14a). Next, G-code (which including the tool paths) was generated using *Slic3r* open source 3D slicing software in *Repetier-Host* 3D printing software, as shown in Fig. 14b. After G-codes were obtained, the models were 3D printed using rubber ink BN-3 (Fig. 14c). It is noted that 3D structures have an uneven surface at some points on the top layer. It was caused by the tackiness of the ink following the nozzle tip as the printing stopped and the printing head was retracted from the printed part. For example, there were many 'stop' positions for printing to move to the next printing location in the last several layers of the

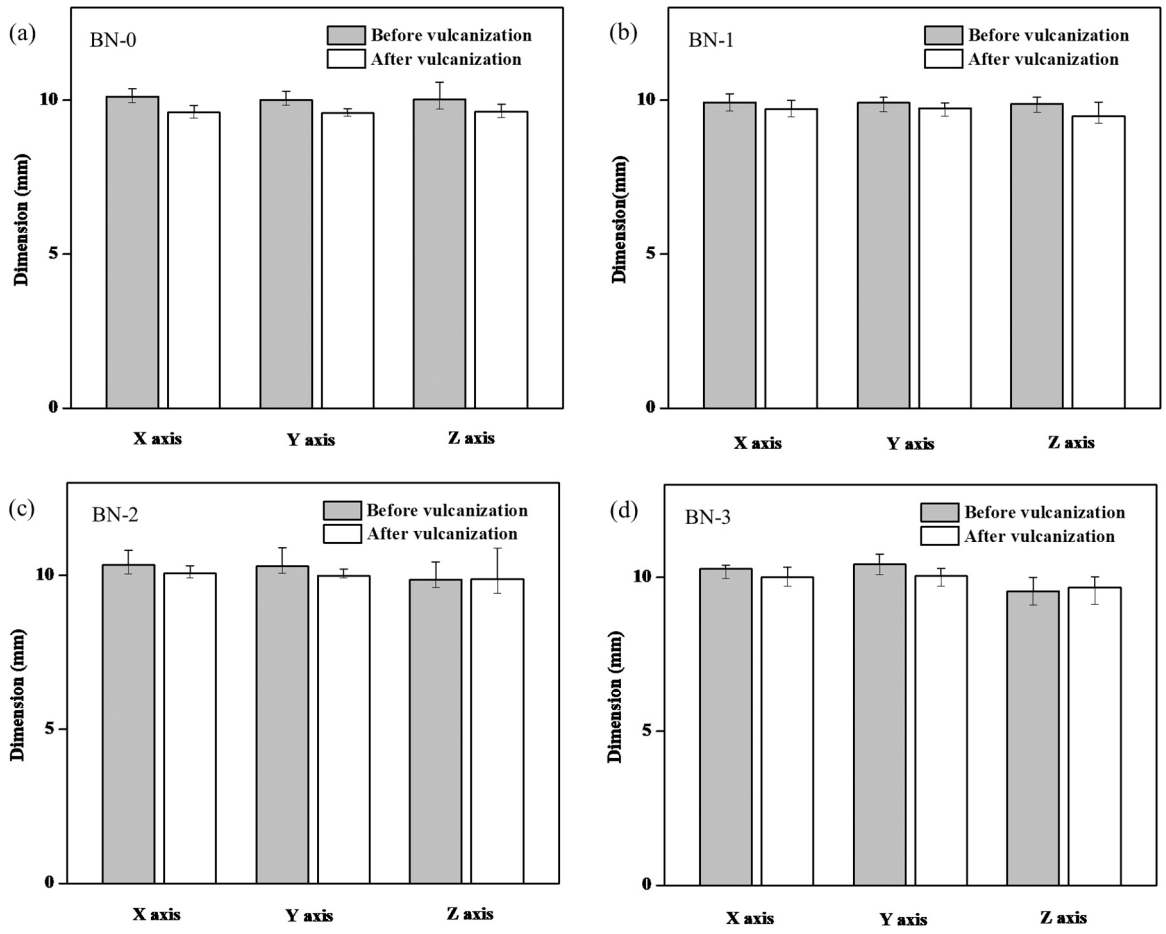

Fig. 11. Dimensional accuracy for parts printed using (a) BN-0, (b) BN-1, (c) BN-2, and (d) BN-3.

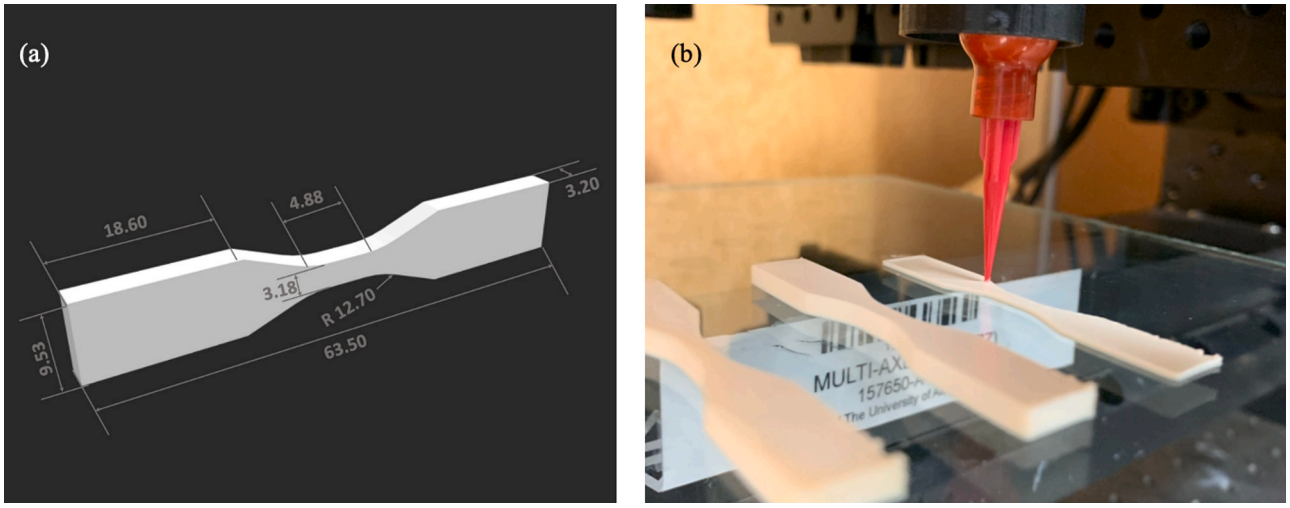

Fig. 12. ASTMD-638 Type V dogbone specimen used for tensile tests: (a) 3D model (dimensions in mm), (b) printing of the specimens.

tread shape (Fig. 14c), resulting in many uneven surfaces compared to the other structures. The printed 3D structures were vulcanized (via heat treatment carried out at 160 °C for 20 min), and the resulting vulcanized parts are shown in Fig. 14d. The successful 3D printing of the design models demonstrates that the prepared rubber ink can be used in future applications using the DP process.

3.7. Discussion

Although a 100% infill density was used, there is always a probability that air gaps (or pores) can be generated. To confirm this, microscopy images of the broken tensile specimens for all four formulations were taken (Fig. S1 in Supplementary Materials). It was found that air gaps existed and were regularly distributed. It is thought that these air gaps were generated after dispensing because of the

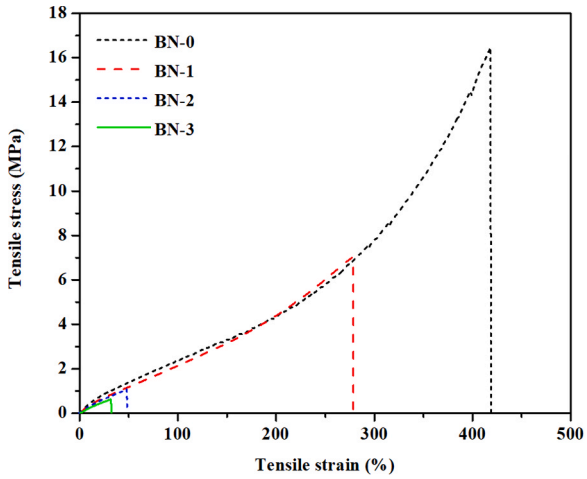

Fig. 13. Stress–strain curves for specimens printed using the rubber inks.

circular shape of a filament, which can't fill the space between the adjacent filaments. Regularly distributed air gaps support this reason, too. The extruded material from the nozzle may flow slightly but there would be limited spreading to fill the gaps due to the shear thinning property. This issue could be partially solved by using a smaller size of a tip and layer height.

One of rubber applications would be tire tread, where tread materials used for commercial tires have the tensile stress of ~16 ~ 19 MPa and elongation at the break of 280 ~580% [46]. It is expected that enhancing the printing process to reduce air gaps and achieving better crosslinking between different rubber types would make the developed rubbers to be used in real applications.

In addition, surface roughness analysis for printed samples was accomplished and data is included in Supplementary Materials (Fig. S2). Ra values on the top surface for 90°, 45°, and 0° against the printing direction are ~63.1 μm, ~51.2 μm, and ~55.2 μm, respectively. An average Ra value on all four sides is 34.4 μm, where the roughness was measured along the build direction. These surface roughness values are not surprisingly high when one considers that the dispensing tip and its size directly affect these values.

Latex has several drawbacks in nature to be used in additive manufacturing. The colloidal state of latex could be easily aggregated under small shear strain and minute change of pH, etc. Latex is regarded as a difficult material in terms of altering its liquid state while sustaining the colloidal state. The prepared rubber inks have a short shelf life without a closed environment since the latex is sensitive to air and temperature that can initiate hardening of them. In addition, the particle size and distribution might be changed from the raw natural rubber latex through the centrifugation and filtration processes, which affect clogging and material properties. Future work will include further investigations on materials and their properties affecting 3D printability and mechanical properties.

4. Conclusions

This study shows the potential for NL as an ink for the direct printing technique. Centrifuged NL, which has a higher amount of solids than natural latex, was shown to have sufficient viscosity to be used as an ink for additive manufacturing using the DP process. It was also verified that liquid rubber can be used to enhance the amount of solid in latex, which can influence the rheological properties and printability of the rubber ink. The printability assessment shows that pressure and speed used in DP can affect the print quality. An experiment conducted to investigate the curing process by BN-3 has shown that the rubber ink was successfully vulcanized. After identifying the curing condition and optimizing the print parameters, 3D structures were printed using the DP process to demonstrate the capability of the developed printable ink. Dimensional accuracy testing of cube specimens shows that the ink with the highest

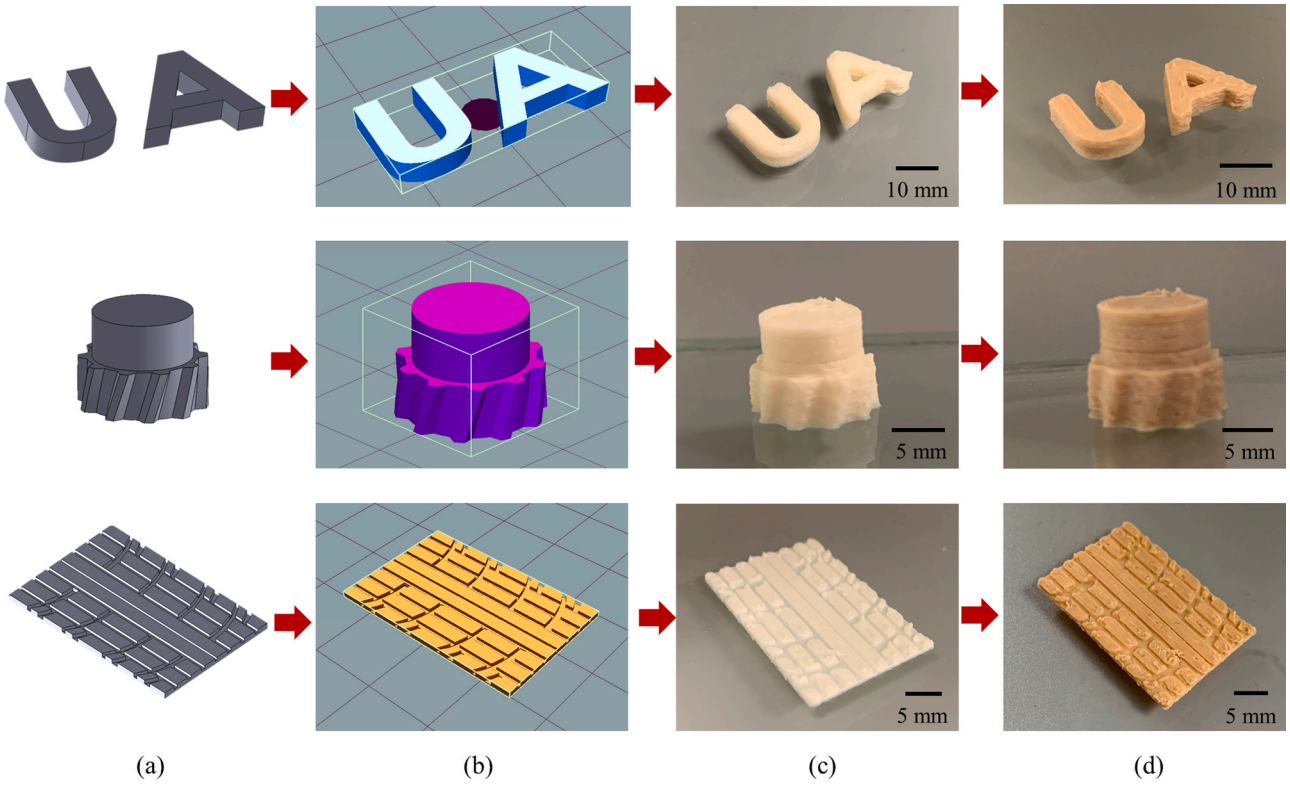

Fig. 14. 3D Structures fabricated by DP using BN-3 rubber ink: (a) CAD models designed in SolidWorks®, (b) tool paths created using a slicing program, (c) 3D printed green parts, and (d) final vulcanized parts.

amount of liquid rubber showed greater dimensional accuracy following vulcanization due to the lower amount of shrinkage. However, tensile test results showed that the stretchability and maximum tensile strength decreased as the amount of liquid rubber in the ink is increased. This study serves as a preliminary study of a printable natural rubber. Our future work will include 1) investigations on effects of temperature and humidity on shelf life and printability; 2) understanding effects of properties of ink formulations on 3D printability and mechanical properties.

CRediT authorship contribution statement

Jae-Won Choi: Conceptualization, Methodology development, Writing - review & editing, Supervision. **Myoeum Kim:** Methodology, Investigation, Writing - original draft, Writing - review & editing, Visualization.

Declaration of Competing Interest

The authors declare that they have no known competing financial interests or personal relationships that could have appeared to influence the work reported in this paper.

Acknowledgements

This work was partially supported by research grants from the Center for Tire Research (CenTiRe). The authors would like to thank Mr. Daniel Kye at The University of Akron for the FTIR analysis that was used for verifying the vulcanization process in this study, and Dr. Jeongwoo Lee at Hankook Tire – ATC for the helpful discussions on natural rubber.

Appendix A. Supporting information

Supplementary data associated with this article can be found in the online version at doi:10.1016/j.addma.2021.102023.

References

[1] S. Wiessner, Rheological Behavior and Rubber Processing, Encyclopedia of Polymeric Nanomaterials, Springer, Berlin, Heidelberg, 2015, pp. 1–10, https://doi.org/10.1007/978-3-642-29648-2.
[2] H.S. Jung, S.H. Kwon, H.J. Choi, J.H. Jung, Y.G. Kim, Magnetic carbonyl iron/natural rubber composite elastomer and its magnetorheology, Compos. Struct. 136 (2016) 106–112, https://doi.org/10.1016/j.compstruct.2015.10.008.
[3] J. Wu, W. Xing, G. Huang, H. Li, M. Tang, S. Wu, Y. Liu, Vulcanization kinetics of graphene/natural rubber nanocomposites, Polymer 54 (13) (2013) 3314–3323, https://doi.org/10.1016/j.polymer.2013.04.044.
[4] P. Tekasakul, S. Tekasakul, Environmental problems related to natural rubber production in Thailand, Earozoru Kenkyu 21 (2) (2006) 122–129, https://doi.org/10.11203/jar.21.122.
[5] S. Rooj, G.C. Basak, P.K. Maji, A.K. Bhowmick, New route for devulcanization of natural rubber and the properties of devulcanized rubber, J. Polym. Environ. 19 (2) (2011) 382–390, https://doi.org/10.1007/s10924-011-0293-5.
[6] Y. Obata, S. Kawabata, H. Kawai, Mechanical properties of natural rubber vulcanizates in finite deformation, J. Polym. Sci. Part A-2 Polym. Phys. 8 (6) (1970) 903–919, https://doi.org/10.1002/pol.1970.160080607.
[7] K. Cornish, Biochemistry of natural rubber, a vital raw material, emphasizing biosynthetic rate, molecular weight and compartmentalization, in evolutionarily divergent plant species, Nat. Prod. Rep. 18 (2) (2001) 182–189, https://doi.org/10.1039/A902191D.
[8] T. Schmidt, A. Hillebrand, D. Wurbs, D. Wahler, M. Lenders, C. Schulze Gronover, D. Prüfer, Molecular cloning and characterization of rubber biosynthetic genes from taraxacum koksaghyz, Plant Mol. Biol. Report. 28 (2) (2010) 277–284, https://doi.org/10.1007/s11105-009-0145-9.
[9] C. Bulei, M.P. Todor, T. Heput, I. Kiss, Directions for material recovery of used tires and their use in the production of new products intended for the industry of civil construction and pavements, IOP Conf. Ser. Mater. Sci. Eng. 294 (2018), 012064, https://doi.org/10.1088/1757-899X/294/1/012064.
[10] V. González, F.J. Martínez-Boza, C. Gallegos, A. Pérez-Lepe, A. Páez, A study into the processing of bitumen modified with tire crumb rubber and polymeric additives, Fuel Process. Technol. 95 (2012) 137–143, https://doi.org/10.1016/j.fuproc.2011.11.018.
[11] R. Singh, R. Singh, J.S. Dureja, I. Farina, F. Fabbrocino, Investigations for dimensional accuracy of Al alloy/Al-MMC developed by combining stir casting and ABS replica based investment casting, Compos. Part B Eng. 115 (2017) 203–208, https://doi.org/10.1016/j.fuproc.2011.11.018.
[12] S.C. Joshi, A.A. Sheikh, 3D printing in aerospace and its long-term sustainability, Virtual Phys. Prototyp. 10 (4) (2015) 175–185, https://doi.org/10.1080/17452759.2015.1111519.
[13] D. Böckin, A.-M. Tillman, Environmental assessment of additive manufacturing in the automotive industry, J. Clean. Prod. 226 (2019) 977–987, https://doi.org/10.1016/j.jclepro.2019.04.086.
[14] M. Savastano, C. Amendola, F. D'Ascenzo, E. Macaroni, 3-D printing in the spare parts supply chain: an explorative study in the automotive industry, in: L. Caporarello, F. Cesaroni, R. Giesecke, M. Missikoff (Eds.), Digitally Supported Innovation, Springer, New York, 2016, pp. 153–170, https://doi.org/10.1007/978-3-319-40265-9.
[15] S.S.L. Chan, R.M. Pennings, L. Edwards, G.V. Franks, 3D printing of clay for decorative architectural applications: effect of solids volume fraction on rheology and printability, Addit. Manuf. 35 (2020), 101335, https://doi.org/10.1016/j.addma.2020.101335.
[16] E. MacDonald, R. Salas, D. Espalin, M. Perez, E. Aguilera, D. Muse, R. Wicker, 3D printing for the rapid prototyping of structural electronics, IEEE Access 2 (2014) 234–242, https://doi.org/10.1109/ACCESS.2014.2311810.
[17] Q. Wei, H. Li, G. Liu, Y. He, Y. Wang, Y.E. Tan, D. Wang, X. Peng, G. Yang, N. Tsubaki, Metal 3D printing technology for functional integration of catalytic system, Nat. Commun. 11 (1) (2020) 4098, https://doi.org/10.1038/s41467-020-17941-8.
[18] V. Chahal, R.M. Taylor, A review of geometric sensitivities in laser metal 3D printing, Virtual Phys. Prototyp. 15 (2) (2020) 227–241, https://doi.org/10.1080/17452759.2019.1709255.
[19] C. Sun, X. Tian, L. Wang, Y. Liu, C.M. Wirth, J. Günster, D. Li, Z. Jin, Effect of particle size gradation on the performance of glass-ceramic 3D printing process, Ceram. Int. 43 (1, Part A) (2017) 578–584, https://doi.org/10.1016/j.ceramint.2016.09.197.
[20] M. Faes, H. Valkenaers, F. Vogeler, J. Vleugels, E. Ferraris, Extrusion-based 3D printing of ceramic components, Procedia CIRP 28 (2015) 76–81, https://doi.org/10.1016/j.procir.2015.04.028.
[21] Y. Yang, Y. Chen, Y. Wei, Y. Li, 3D printing of shape memory polymer for functional part fabrication, Int. J. Adv. Manuf. Technol. 84 (9) (2016) 2079–2095, https://doi.org/10.1007/s00170-015-7843-2.
[22] C.X.F. Lam, X.M. Mo, S.H. Teoh, D.W. Hutmacher, Scaffold development using 3D printing with a starch-based polymer, Mater. Sci. Eng. C 20 (1) (2002) 49–56, https://doi.org/10.1016/S0928-4931(02)00012-7.
[23] G. Postiglione, G. Natale, G. Griffini, M. Levi, S. Turri, Conductive 3D microstructures by direct 3D printing of polymer/carbon nanotube nanocomposites via liquid deposition modeling, Compos. Part A Appl. Sci. Manuf. 76 (2015) 110–114, https://doi.org/10.1016/j.compositesa.2015.05.014.
[24] D. Kokkinis, M. Schaffner, A.R. Studart, Multimaterial magnetically assisted 3D printing of composite materials, Nat. Commun. 6 (1) (2015) 8643, https://doi.org/10.1038/ncomms9643.
[25] P. Dudek, FDM 3D printing technology in manufacturing composite elements 58 (4) (2013) 1415–1418, https://doi.org/10.2478/amm-2013-0186.
[26] G. Brunello, S. Sivolella, R. Meneghello, L. Ferroni, C. Gardin, A. Piattelli, B. Zavan, E. Bressan, Powder-based 3D printing for bone tissue engineering, Biotechnol. Adv. 34 (5) (2016) 740–753, https://doi.org/10.1016/j.biotechadv.2016.03.009.
[27] D.-T. Chou, D. Wells, D. Hong, B. Lee, H. Kuhn, P.N. Kumta, Novel processing of iron–manganese alloy-based biomaterials by inkjet 3-D printing, Acta Biomater. 9 (10) (2013) 8593–8603, https://doi.org/10.1016/j.actbio.2013.04.016.
[28] J. Mueller, K. Shea, C. Daraio, Mechanical properties of parts fabricated with inkjet 3D printing through efficient experimental design, Mater. Des. 86 (2015) 902–912, https://doi.org/10.1016/j.matdes.2015.07.129.
[29] M.P. Browne, M. Pumera, Impurities in graphene/PLA 3D-printing filaments dramatically influence the electrochemical properties of the devices, Chem. Commun. 55 (58) (2019) 8374–8377, https://doi.org/10.1039/C9CC03774H.
[30] Z. Weng, J. Wang, T. Senthil, L. Wu, Mechanical and thermal properties of ABS/montmorillonite nanocomposites for fused deposition modeling 3D printing, Mater. Des. 102 (2016) 276–283, https://doi.org/10.1016/j.matdes.2016.04.045.
[31] X. Fu, X. Zhang, Z. Huang, Axial crushing of Nylon and Al/Nylon hybrid tubes by FDM 3D printing, Compos. Struct. 256 (2021), 113055, https://doi.org/10.1016/j.compstruct.2020.113055.
[32] M. Kim, D.G. Philip, M.O.F. Emon, J.-W. Choi, Effects of hardness on the sensitivity and load capacity of 3D Printed sensors, Int. J. Precis. Eng. Manuf. 22 (2021) 483–494, https://doi.org/10.1007/s12541-020-00468-9.
[33] B.A. Wolf, Shear thinning: determination of zero-shear viscosities from measurements in the non-newtonian region, Macromol. Chem. Phys. 221 (14) (2020), 2000130, https://doi.org/10.1002/macp.202000130.
[34] N.G. Tanikella, B. Wittbrodt, J.M. Pearce, Tensile strength of commercial polymer materials for fused filament fabrication 3D printing, Addit. Manuf. 15 (2017) 40–47, https://doi.org/10.1016/j.addma.2017.03.005.
[35] A. Kulkarni, G.D. Soraru, J.M. Pearce, Polymer-derived SiOC replica of material extrusion-based 3-D printed plastics, Addit. Manuf. 32 (2020), 100988, https://doi.org/10.1016/j.addma.2019.100988.
[36] S. Singh, R. Signh, Mechanical characterization and comparion of additive manufactured ABS PolyflexTM ABS/PolyflexTM blended functional prototypes, Rapid Prototyp. J. 26 (2) (2020) 225–237, https://doi.org/10.1108/RPJ-11-2017-0234.
[37] M. Lukie, J. Clarke, C. Tuck, W. Whittow, G. Wells, Printaility of elastomer latex for additive manufacturing or 3D printing, J. Appl. Polym. Sci. 133 (4) (2016), https://doi.org/10.1002/app.42931, 42931–42931.

[38] M.A.Q. Santiago, C.L. Hedegaard, J.R.C. Pita, Additive manufacturing with liquid latex and recycled end-of life rubber, 3D Print. Addit. Manuf. 6 (3) (2019) 149–157, https://doi.org/10.1089/3dp.2018.0062.
[39] P.J. Scott, W. Meenakshisundaram, M. Hegde, G.R. Kasprzak, C.R. Winkler, K. D. Feller, C.B. Williams, T.E. Long, 3D printing latex: a route to complex geometries of high molecular weight polymers, ACS Appl. Mater. Sci. 12 (2020) 10918–10928, https://doi.org/10.1021/acsami.9b19986.
[40] Q. Sun, J. Liu, H. Cheng, Y. Mou, J. Liu, Y. Peng, M. Chen, Fabrication of 3D structures via direct ink writing of kaolin/graphene oxide composite suspensions at ambient temperature, Ceram. Int. 45 (15) (2019) 18972–18979, https://doi.org/10.1016/j.ceramint.2019.06.136.
[41] F. Abdeljawad, D.S. Bolintineanu, A. Cook, H. Brown-Shaklee, C. DiAntonio, D. Kammler, A. Roach, Sintering processes in direct ink write additive manufacturing: a mesoscopic modeling approach, Acta Mater. 169 (2019) 60–75, https://doi.org/10.1016/j.actamat.2019.01.011.
[42] A. Cosgrove, L. Lopez, J. Hernandez-Ortiz, T. Osswald, E. Camacho, Modeling the vulcanization process of high consistency rubber and liquid silicone rubber, Soc. Plast. Eng. (2004) 953–957 (ANTEC. conference proceedings), http://citeseerx.ist.psu.edu/viewdoc/download?doi=10.1.1.522.4090&rep=rep1&type=pdf.
[43] R.M. Saeed, J.P. Schlegel, C. CastaÒo, R. Sawafta, Uncertainty of thermal characterization of phase change material by differential scanning calorimetry analysis, Int. J. Eng. Res. Technol. 5 (1) (2016) 405–412. https://www.ijert.org/research/uncertainty-of-thermal-characterization-of-phase-change-material-by-differential-scanning-calorimetry-analysis-IJERTV5IS010381.pdf.
[44] F.J. Galindo-Rosales, F.J. Rubio-Hernández, J.F. Velázquez-Navarro, Shear-thickening behavior of Aerosil® R816 nanoparticles suspensions in polar organic liquids, Rheol. Acta 48 (6) (2009) 699–708, https://doi.org/10.1007/s00397-009-0367-7.
[45] H. Hingorani, Y.-F. Zhang, B. Zhang, A. Serjouei, Q. Ge, Modified commercial UV curable elastomers for passive 4D printing, Int. J. Smart Nano Mater. 10 (3) (2019) 225–236, https://doi.org/10.1080/19475411.2019.1591540.
[46] M. Bijarimi, Z. Hassan, M.D.H. Beg, Mechanical properties of industrial tyre rubber compounds, J. Appl. Sci. 10 (13) (2010) 1345–1348, https://doi.org/10.3923/jas.2010.1345.1348.